Received: 16 February 2022 | Accepted: 3 August 2022

DOI: 10.1002/jcp.30857

RESEARCH ARTICLE

Journal of Cellular Physiology WILEY

How to follow lipid droplets dynamics during adipocyte metabolism

Nadav Kislev | Shira Eidelheit | Shaked Perlmutter | Dafna Benayahu

Department of Cell and Developmental Biology, Sackler School of Medicine, Tel Aviv University, Tel Aviv, Israel

Correspondence
Dafna Benayahu, Department of Cell and Developmental Biology, Sackler School of Medicine, Tel Aviv University, Tel Aviv 6997801, Israel.
Email: dafnab@tauex.tau.ac.il

Abstract

Lipid droplets (LDs) are important cellular organelles due to their ability to accumulate and store lipids. LD dynamics are associated with various cellular and metabolic processes. Accurate monitoring of LD's size and shape is of prime importance as it indicates the metabolic status of the cells. Unintrusive continuous quantification techniques have a clear advantage in analyzing LDs as they measure and monitor the cells' metabolic function and droplets over time. Here, we present a novel machine-learning-based method for LDs analysis by segmentation of phase-contrast images of differentiated adipocytes (in vitro) and adipose tissue (in vivo). We developed a new workflow based on the ImageJ waikato environment for knowledge analysis segmentation plugin, which provides an accurate, label-free, live single-cell, and organelle quantification of LD-related parameters. By applying the new method on differentiating 3T3-L1 cells, the size of LDs was analyzed over time in differentiated adipocytes and their correlation with other morphological parameters. Moreover, we analyzed the LDs dynamics during catabolic changes such as lipolysis and lipophagy and demonstrated its ability to identify different cellular subpopulations based on their structural, numerical, and spatial variability. This analysis was also implemented on unstained ex vivo adipose tissues to measure adipocyte size, an important readout of the tissue's metabolism. The presented approach can be applied in different LD-related metabolic conditions to provide a better understanding of LD biogenesis and function in vivo and in vitro while serving as a new platform that enables rapid and accurate screening of data sets.

KEYWORDS

adipocyte metabolism, adipose tissue, lipid droplets, lipolysis

1 | INTRODUCTION

Lipid droplets (LDs) are organelles that play an important role in energy metabolism through their ability to accumulate and store lipids. Although most mammalian cell types can store lipids in LDs, the primary lipid pool resides in adipose tissue adipocytes (Farese & Walther, 2009; Olzmann & Carvalho, 2019; Onal et al., 2017). Adipocytes are specialized in their ability to store energy like triglycerides in the form of LDs in a process termed lipogenesis. This biogenesis process lies in the center of adipogenesis as

differentiation of preadipocytes to adipocytes is characterized by the accumulation of LDs (Tang & Lane, 2012). Upon stimulation, catalytic lipolytic enzymes break the LD down to provide an energy substrate in times of need, thus maintaining the needed balance in lipid homeostasis (Ducharme & Bickel, 2008). The degradation of LDs appears in the form of lipophagy or lipolysis. While neutral cytosolic lipolysis relies on LD-associated lipases, lipophagy is based on a lysosomal-autophagic pathway; they both play a crucial role in adipocyte metabolism (Zechner et al., 2017). In vitro adipogenesis-based cell cultures are frequently utilized as a model system in LD biogenesis and dynamics research, with 3T3-L1 cells often being used as a model for adipocytes function (Novikoff et al., 1980).

Tracking and quantifying intracellular LDs can be applied using various techniques that differ in their approach. They include various staining methods that utilize lipophilic probes such as Nile red, Oil-red O, and BODIPY to provide a snapshot of the LDs morphology. Some staining techniques require fixation of the culture, thus neutralizing the ability to monitor the LDs biogenesis over time, which leads to the loss of valuable data (Listenberger & Brown, 2007). Other methods use phase-contrast image processing to identify, measure and quantify LDs in the same culture over time. Our group has previously developed several methods to pursue an accurate monitoring technique of adipocyte function through morphological analysis of their LDs parameters (Lustig et al., 2019; Shoham et al., 2012). These methods were used to quantify both macro and micro-scale changes in LDs of adipocytes and correlate them with adipogenesis. The primary advantage of a noninvasive imaging tool lies in its ability to produce continuous and coordinated analyses on the same cultures and integrate them with other assays and tools, allowing us to follow metabolic processes in adipocytes under various treatments and conditions.

LD dynamics are also associated with several metabolic conditions, making them an important analysis target. Both excessive and insufficient storage capacities of LDs are related to metabolic pathologies such as atherosclerosis, fatty liver disease, lipodystrophy, insulin resistance, diabetes, and obesity (Greenberg et al., 2011; Krahmer et al., 2013; Onal et al., 2017). Adipose tissue dysfunction is characterized by the expansion of adipocytes due to excessive caloric intake (Guilherme et al., 2008). The measurement of individual adipocytes is key in determining the adiposity of the tissue and its metabolic health. Thus, accurate and dynamic measurements of the morphological alteration in LDs in vivo are of great importance (Laforest et al., 2015).

In this study, we have developed an advanced approach to quantify LD dynamics using an ImageJ-based supervised machine-learning segmentation tool based on the Trainable waikato environment for knowledge analysis (WEKA) segmentation (Arganda-Carreras et al., 2017; Schindelin et al., 2012). This method aims to create a robust analysis based on segmentation that allows measuring large sets continuously with live imaging of single-cell dynamics. For this purpose, we used the plugin that segments phase-contrast images to different classes, including LDs, based on the measured organelles' morphology. Once a satisfactory segmentation product was built, it was applied to several sets of images, enabling us to rapidly analyze large data sets, which can be useful for screening analyses of therapeutic and pharmaceutical agents. After comparing a thresholding technique to validate our method, we used it to study the LDs dynamics and subpopulations in adipocytes in vitro and on adipose tissue. Since LD morphology is strongly related to essential metabolic processes, the ability to measure the dynamics of LDs robustly and accurately makes the presented method of segmentation analysis a vital tool in investigating adipocyte differentiation and function.

2 | MATERIALS AND METHODS

2.1 | In vitro cell culture analysis

Mouse embryonic 3T3-L1 pre-adipocytes (American Type Culture Collection) were cultured and differentiated over a period of 3 weeks, as was previously described (Mor-Yossef Moldovan et al., 2019, 2020). For the lipolysis induction, 10 μM of forskolin (Peprotech) was added to the maintenance medium; the forskolin was kept for 2 h. For the lysosomal-autophagic pathway induction, 5 mM of metformin was added to a Dulbecco's modified Eagle's medium without glucose for 1 h (Biological Industries) for a total of 8 h. To follow the acidic compartments in the cells, 100 nM of LysoTracker Green (Life Technologies) was added to the last hour of the experiment.

2.2 | Level of adipogenesis (LOA)

The LOA was calculated as previously described (Lustig et al., 2019). Shortly, Stitched phase-contrast ×40 images of differentiated cultures were taken at different points throughout adipogenesis in the EVOS FL Auto 2 microscope (Invitrogen). Based on the major visual difference between fibroblasts and adipocytes, a visual difference mapping was obtained. This map was used to calculate the LOA in each culture.

2.3 | LD quantification

EVOS FL Auto 2 microscope (Invitrogen) was used to take phase-contrast and fluorescent images in ×200 magnification of cultured 3T3-L1 cells throughout differentiation for all LD-related analyses (cell growth, morphology, and LDs accumulation). For the lipolysis assay, time-lapsed images were taken every 15 min postinduction for 2 h.

2.4 | Machine learning segmentation

To define the LDs accurately, we used the FIJI ImageJ (NIH) plugin, named trainable WEKA segmentation (Arganda-Carreras

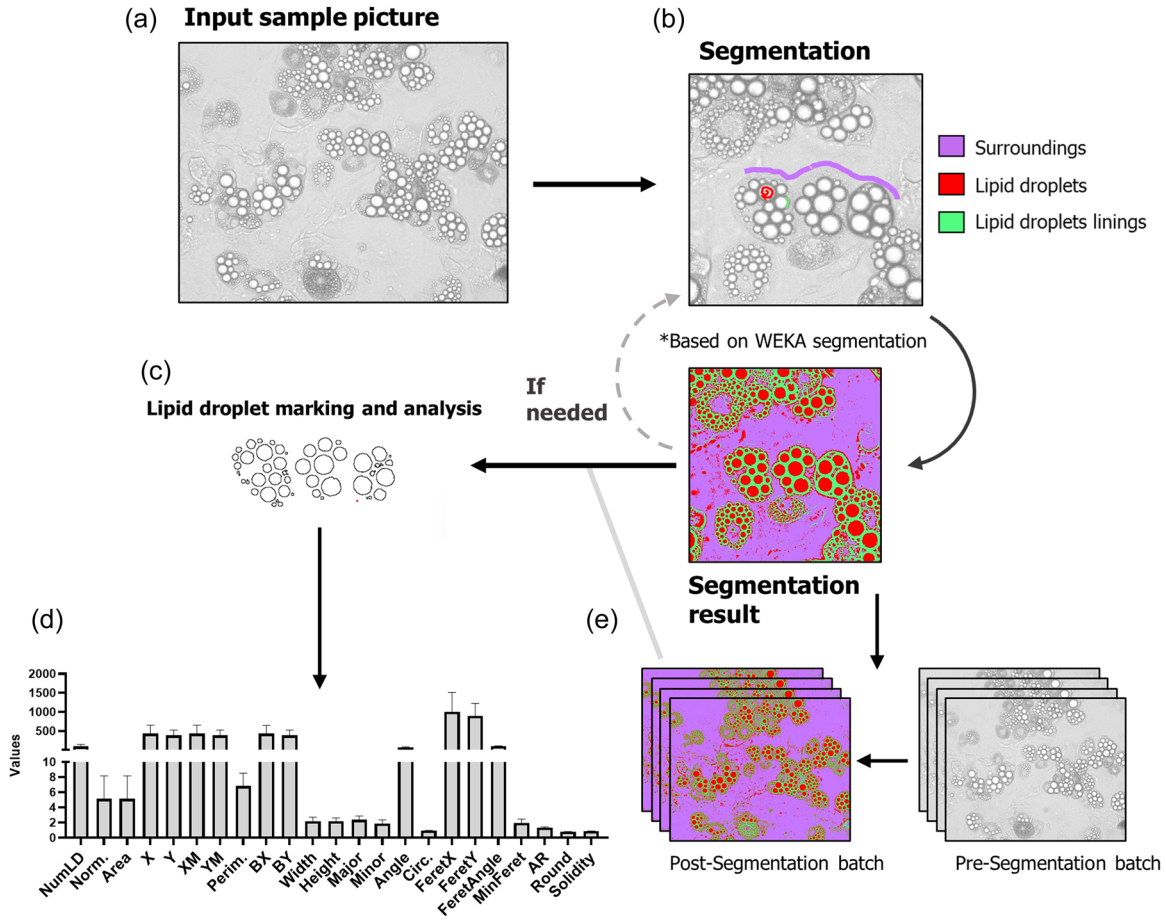

FIGURE 1 Lipid droplet (LD) quantification workflow. (a) Input sample phase-contrast image of differentiating 3T3-L1 cells. (b) Segmentation process using waikato environment for knowledge analysis (WEKA) trainable segmentation tool. Three classes were assigned (red—droplet content, green—LD linings, purple—surroundings). The classifier was trained until a satisfactory product was produced. (c) LDs were obtained from the binary segmented image using ImageJ's automatic analyze particles tool. (d) The droplets were analyzed for all available morphologic variables (e) the classifier can be applied to other images to obtain batches of binarized LDs images.

et al., 2017). Figure 1a shows a representative image that was utilized to create the analysis classifier for all other images. Three classes were defined and allocated to the different parts of the picture, purple represents the surroundings, red represents the LDs, and green is the outline of the droplet (Figure 1b). Each time the classifier is "trained," the parts that were not recognized correctly were redefined, and this step was repeated until the segmentation was satisfactory (Figure 1b). The classifier can be applied to the same image to generate a binary image with markable and quantifiable LDs (Figure 1c,d) and can be applied on additional images (Figure 1e). The marked LDs were added to the region of interest (ROI) with the analyze particles option. Non-LD particles can be filtered by applying circularity and size thresholds to the images if needed. To generate a cell-based analysis, the perimeter of the cell was manually marked and then measured by the analyze particles option. *Thresholding*: images were converted into an 8-bit grayscale thresholded and analyzed with "analyze particles."

2.5 | 3D segmentation analysis

EVOS FL Auto 2 microscope (Invitrogen) was used to take Z-stack phase-contrast images in ×200 magnification of differentiated 3T3-L1 cells; a 3D trainable WEKA segmentation tool was then used to segment the Z stack images to generate binary stacks (Arganda-Carreras et al., 2017). Supporting Information: Figure S1a shows a representative set of Z stack images utilized to create the analysis classifier for all other images. A 3D surface plot constructed from the Z-stack simulates the cell's structure. Since images in the stack have different morphological attributes, only two classes were defined and allocated to the different parts of the picture, red represents the LDs, and green is the outline of the droplet. Each time the classifier is "trained," the parts that were not recognized correctly were redefined, and this step was repeated until the segmentation was satisfactory. The classifier can be applied to the same image to generate a binary image with markable and quantifiable LDs and can be applied to additional images (Supporting Information: Figure S1b).

To generate a cell-based analysis, the perimeter of the cell was manually marked, and its surroundings were cleared. For the LDs 3D quantification analysis, the 3D object counter tool was used as it generates 3D-related parameters (Bolte & Cordelières, 2006).

2.6 | Ex vivo adipose tissue analysis

Epididymal visceral adipose tissues (VAT) were taken from C57bl/6J mice. The mice were kept in a conventional facility with 12 h light/dark cycles and were fed with standard chow and provided water ad libitum, according to guidelines of the IACUC Approval (01-21-044). Whole-mount images of VAT were taken by a confocal microscope (Leica SP8; Leica) in ×200 magnification (Kislev et al., 2021). The images were segmented using the WEKA trainable segmentation tool with two classes (red = adipocytes, green = linings); after a satisfactory product was achieved, a watershed filter was added to connect missing adipocytes. The cells were quantified using the analyze particles tool.

2.7 | Statistical analysis

Analysis was performed using GraphPad Prism v.9.1.1 and Rstudio. The results are presented as means ± SD. All results were tested for normal distribution by Kolmogorov–Smirnov test, and outliers were identified using the ROUT method. Statistical differences comparing the mean values were tested using two-tailed, unpaired *t*-tests, one-way analysis of variance (ANOVA), or two-way ANOVA where appropriate. Values that were not normally distributed were tested using Mann–Whitney or Kruskal–Wallis (for three or more groups) for multiple comparisons. Correlations were tested using nonparametric Spearman's correlation.

3 | RESULTS

3.1 | LD analysis throughout adipogenesis

Differentiated 3T3-L1 cells were monitored at 14- and 21-day post adipogenesis induction to examine their LD-related morphological attributes. The macro analysis was based on whole-culture binary images that displayed the progression of cellular differentiation during the experiment. As shown in Figure 2a, the level of adipogenesis, which summarizes the percentage of the culture filled with adipocytes, was sixfold higher after 21 days compared to 14 days. We then evaluated the progression in LD accumulation of the same cultures at the microscale using the novel segmentation tool that generated analyzable binary images (Figure 2b). The mean LD area increased more than threefold, from 8.65 μm^2 on day 14 to 26.87 μm^2 on day 21, with a change in the distribution of the LDs area (Figure 2c). The results suggest that LDs are monitorable and detectable through the segmentation analysis, with changes in the LDs biogenesis accumulation.

3.2 | Segmentation validation

To validate the efficacy of the segmentation as an LD identifier, it was set up against a thresholding approach. The analysis was performed on the same cells and LDs, enabling us to compare the results of the two methods accurately. As shown in Figure 2d, the segmentation method generated a more accurate image and was able to detect small LDs; even droplets with an incomplete or blurry outline are detectable. The detection efficacy of both methods was then assessed by comparing their LD discovery sensitivity. The number of detectable LDs in each technique was extracted and divided by a manual count of the LDs in the respective cell, which generated a detection ratio for each method. As shown in Figure 2e, the results suggested that the percentage of LDs per cell was fourfold higher when using the segmentation method, suggesting that this approach is more sensitive in detecting LDs.

Interestingly, the quantification of the mean LDs area showed significant differences between the thresholded and segmented LDs, with mean areas of 6.8 and 3.5 μm^2, respectively. To examine the discrepancies between the methods, we compared the distribution of all detected LDs. It was apparent that the segmentation tool found the same number of large LDs as the thresholding tool and noticeably more smaller droplets (Figure 2f). From these findings, we concluded that the new method detects the small droplets more effectively and thus affecting the mean size and absolute quantity of the droplets (Figure 2f). Overall, these results suggest that segmentation analysis provided a more precise quantification of the droplets, with emphasis on small droplets that were undetectable with thresholding, that is, the presented method tracking is more defined, which is crucial in determining the biogenesis of other lipogenic functions more accurately.

Moreover, we then compared the results generated from our 3D analysis to the regular 2D analysis. The 3D analysis is based on Z-stacked phase-contrast images and can be used to measure the volume of LDs, whereas the 2D measures only the area and is based only on one z location. As shown in Supporting Information: Figure S1c, the LDs area measured in 2D are highly correlated ($r = 0.96$) with the LDs volume with a successful identification rate of more than 90% LDs in a cell. The center of mass of each droplet was also measured in every cell. On average, more than 80% of the LDs in each cell share the same center of mass (Supporting Information: Figure S1d), suggesting that a single image might effectively analyze the majority of LDs accurately. We then focused on a group of cells and evaluated their mean LDs area compared to other morphological parameters. The cells were stratified into three groups based on their average LD distribution pattern, with 35 μm^2 < considered large LDs cells and 10 μm^2 > small; all the rest were considered medium LDs sized cells (Figure 2g). The LDs average size

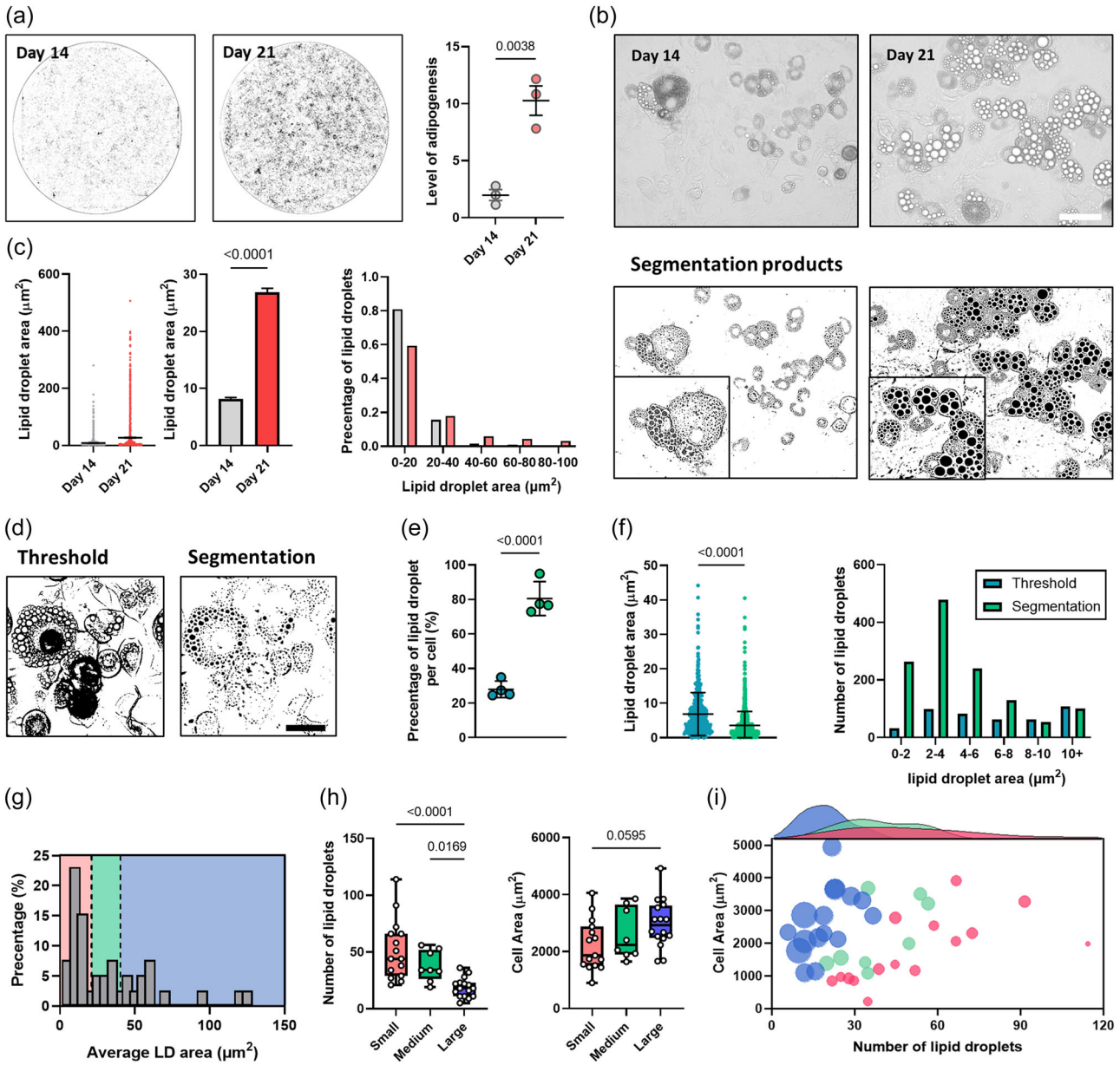

FIGURE 2 Lipid droplet (LD) analysis through segmentation. (a) Representative stitched images of cultured adipocytes and level of adipogenesis analysis ($n = 3$) after 14 (gray) and 21 (red) days post adipogenesis induction. (b) Phase-contrast images and segmentation products of adipocytes after 14 and 21 days post induction (magnification ×200, scale bar = 100 μm). (c) Single LD area distribution after 14 (gray, $n = 2847$) and 21 days (red, $n = 4528$). (d) Representative thresholding and segmentation products of differentiating adipocytes (magnification ×200, scale bar= 50 μm). (e) Percentage of detectable LDs in comparison to manual counting ($n = 4$), by thresholding (blue) and segmentation (green). (f) Single LD area distribution by thresholding (blue, $n = 445$) and segmentation (green, $n = 1264$) tools (g) distribution of adipocytes based on their average LD area ($n = 40$), the cells were divided into three groups, small (red, <10 μm^2), large (blue, >35 μm^2), and medium (green) (h) histograms of the number of LDs, cell area, and average LD size of the small (red), medium (green), and large (blue) averaged LDs area, significance was calculated using unpaired nonparametric Kruskal–Wallis test, followed by Dunn's posttest. (i) Scatter plot of the cell area, and the number of LDs of the small (red), medium (green), and large (blue) groups, the dots' radius corresponds with the average LDs area, together with a distribution plot of the number of LDs. Unless stated otherwise, significance was calculated using an unpaired nonparametric Mann–Whitney test.

correlated with the cell projected area, with large, averaged LD cells exhibiting higher cell areas. The large LDs group had a lower number per cell than the other group, demonstrating the adipogenic propagation heterogeneity (Figure 2h). As shown in Figure 2i, the number of LDs correlates with the average LD size, with the large and small groups generating two distinct clusters based on their number of droplets and the cell's projected area. This single-cell analysis demonstrated the relationship between different morphological parameters and their importance in understanding the heterogeneity of the cells.

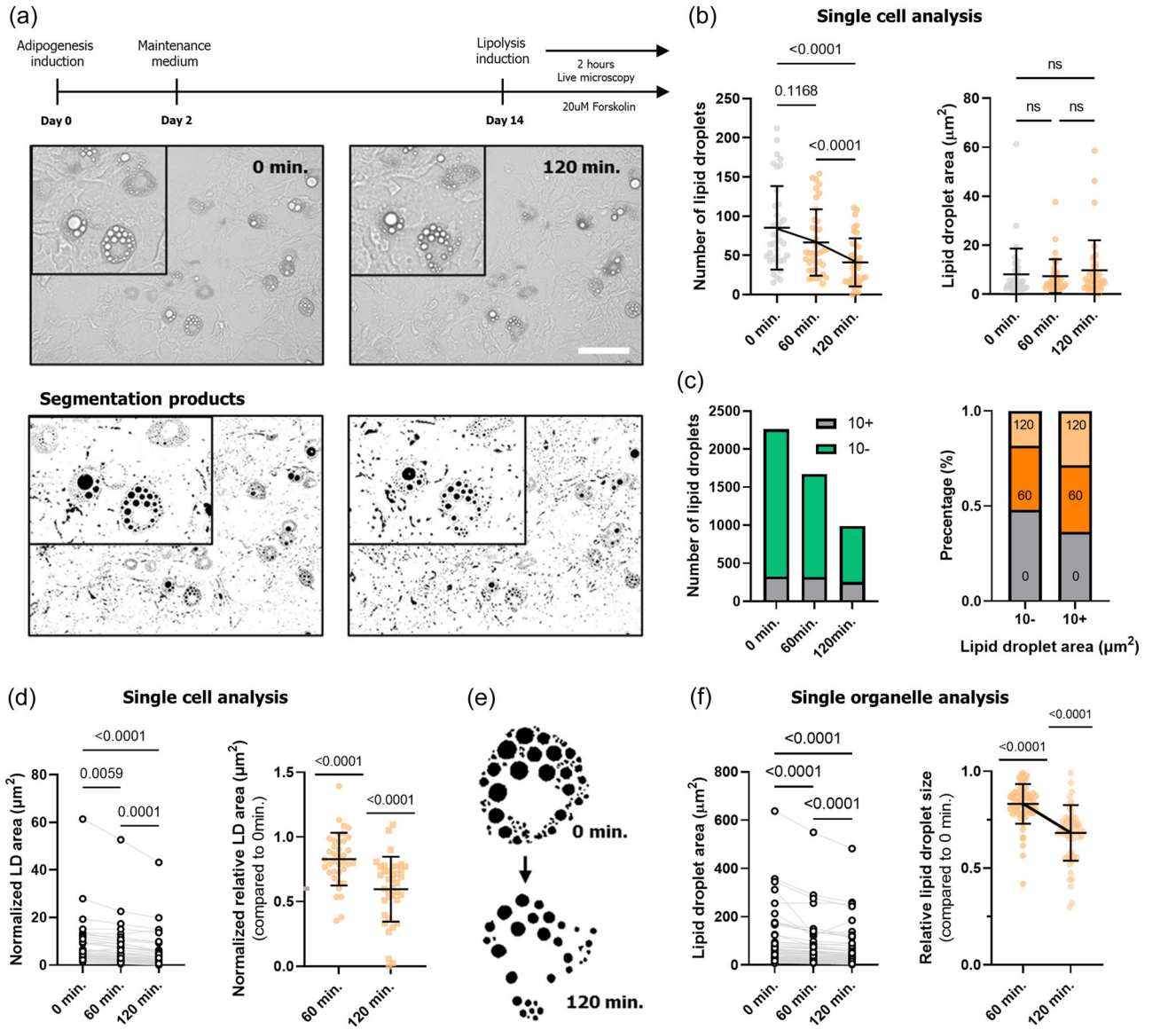

FIGURE 3 Lipid droplet (LD) analysis during lipolysis. (a) The experimental model, and phase contrast images and segmentation products at 0 and 120 min post lipolysis induction (magnification of ×200, scale bar = 100 µm). (b) Number of LDs and LD area per cell after 0 min (gray), 60 and 120 min (orange), $n = 38$, significance was calculated using paired one-way analysis of variance (ANOVA) with Friedman's posttest. (c) Stacked bars of amount of 10− µm LDs (green) and 10+ µm^2 LDs (gray) through lipolysis and the respective percentage of 10− and 10+ µm^2 LDs after 120 min (light orange) 60 min (orange) and 0 min (gray). (d) Paired normalized LD area analysis after 0, 60, and 120 min, and normalized relative (to time 0) LD area analysis after 60 and 120 min, normalization was performed to the initial LD number of a cell, $n = 38$, significance was calculated using paired one-way ANOVA with Friedman's posttest and Wilcoxon signed rank test, respectively. (e) Illustration of a single cell and organelle LDs dynamics during lipolysis. (f) Paired single organelle LD area analysis after 0, 60, and 120 min, and relative (to time 0) LD area analysis after 60 and 120 min, $n = 63$, significance was calculated using paired one-way ANOVA with Friedman's posttest and Wilcoxon signed rank test, respectively.

3.3 | LD analysis during neutral lipolysis

Next, we established a lipolysis detection workflow and employed the segmentation method to generate an imaging analysis, as presented in Figure 3a,e. Lipolysis was induced using 10 µM of forskolin, a cAMP inducer known for its lipolytic induction in adipocytes, for 2 h and images were captured using live imaging. The images were analyzed at 0, 60, and 120min at a single-cell resolution for the LD number and size dynamics. Forskolin lipolysis induction triggered a significant change in LDs per cell, with 50% reduction in the mean LDs count after 2 h. In contrast, quantitative analysis of the average LD area per cell showed no significant differences over time (Figure 3b).

Separating the data to two distinct LD subpopulations based on their size (10± µm^2) revealed that the number of larger LDs over 10+ µm^2 remained unchanged while the lower than 10 µm number

was cut in half, indicating that the reduction in LDs was solely due to the shrinkage and depletion of the smaller size of the subpopulation. To account for the changes in the LDs number, we normalized the cellular data by the initial LDs count of each cell. The normalized data revealed significant changes in the average LD area over time, with a 19% and 35% reduction after 1 and 2 h, respectively (Figure 3d). The segmentation analysis enables us to track the dynamics of individual LDs and study their tendencies over time and different treatments (Figure 3e). The results obtained from the single organelle analysis were in accordance with the normalized results, with significant shrinkage of individual LDs after 2 h (Figure 3f). The lipolysis results demonstrated the ability of the trainable segmentation to detect LDs dynamics accurately and robustly.

3.4 | Stratification of lipolytic adipocytes based on average cellular LD size

To further evaluate the dynamics of lipolysis in adipocytes, the cells were divided into three subpopulations based on their average LD size distribution in the initial time point (Figure 4a). Validation was made with a principal component analysis of averaged morphological parameters for each cell, exhibiting the different clusters based on their average LD size (Figure 4b). The LD depletion rate of the small LD population was substantially greater (Figure 4c), also demonstrated by the significant difference between the small LD population and the other in their relative number of LD (Figure 4d). The normalized relative LD size analysis showed a reduction in LD size only in the small LD subpopulation, indicating that this might be the primary lipolytic adipocyte population in vitro, with the ability to break down its fatty content rapidly. The data acquired from the analysis can be used together with different methods to find novel subpopulations regarding adipocytes and other lipids containing cells.

3.5 | LD analysis during acidic lipolysis

To complete the story focusing on adipocyte metabolism and cellular triacylglycerol catabolism, we established an acidic lipolysis detection workflow that tracks the lysosomal activity in the cells and integrates it with the presented segmentation model. As shown in Figure 5a, acidic lipolysis was induced by combining 5 mM of metformin, an antidiabetic drug that also triggers autophagy, and nutritional restriction (NR) to the cells for 8 h. A fluorescently labeled lysosome tracker (Lysotracker: LysoT) was added to account for the lysosomal activity in the cytoplasm and, more specifically, around the LDs. The metformin+ NR (MetF + NR) treatment triggered a significant change in LysoT intensity compared to untreated cells, with differences in

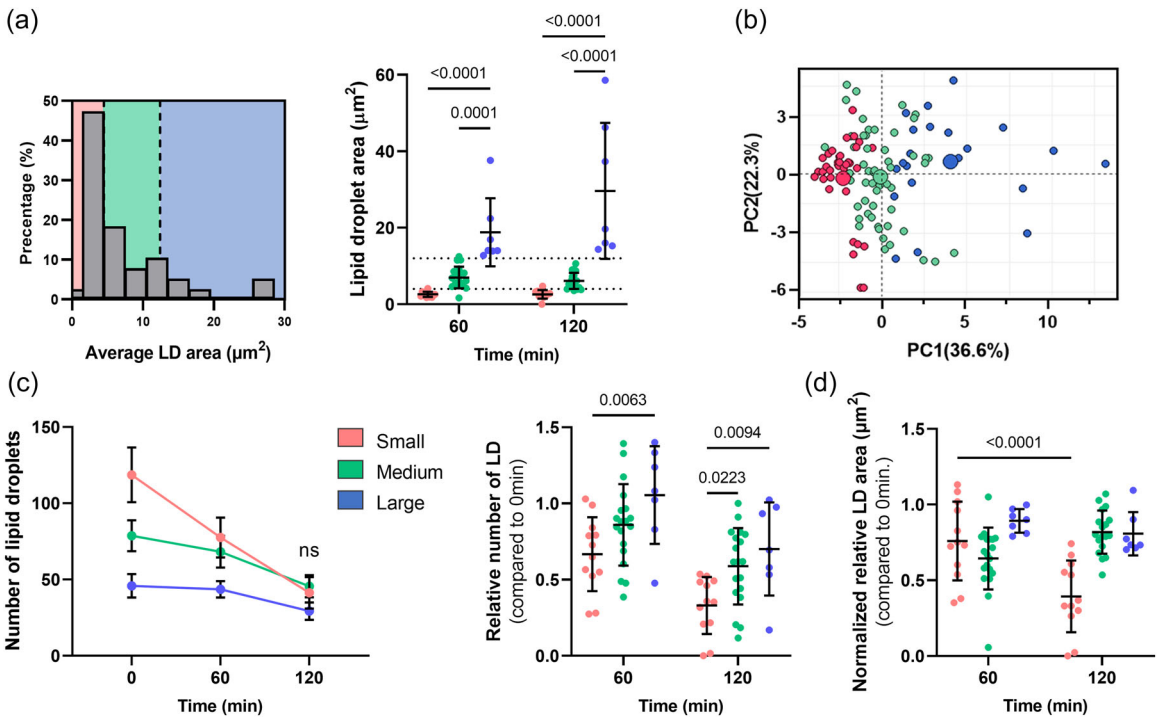

FIGURE 4 Stratification of lipolytic adipocytes based on average cellular lipid droplet (LD) size. (a) Distribution of lipolytic adipocytes in 0min based on their average LD area (n = 38), the cells were divided into three groups, small (red, <3.5 μm^2), large (blue, >15 μm^2), and medium (green), and the averaged LD area after 60 and 120 min of the three groups. (b) Principal component analysis of all morphological parameters of each cell for the small (red), medium(green), large (blue) cells. (c) Number of LDs over time in the small (red), medium(green), large (blue) groups, and the relative number of LD. (d) Normalized relative (to time 0) LD area analysis after 60 and 120 min for the small (red), medium(green), large (blue) groups, normalization was performed to the initial LD number of a cell. Unless stated otherwise, significance was calculated using two-way analysis of variance with Sidak's posttest.

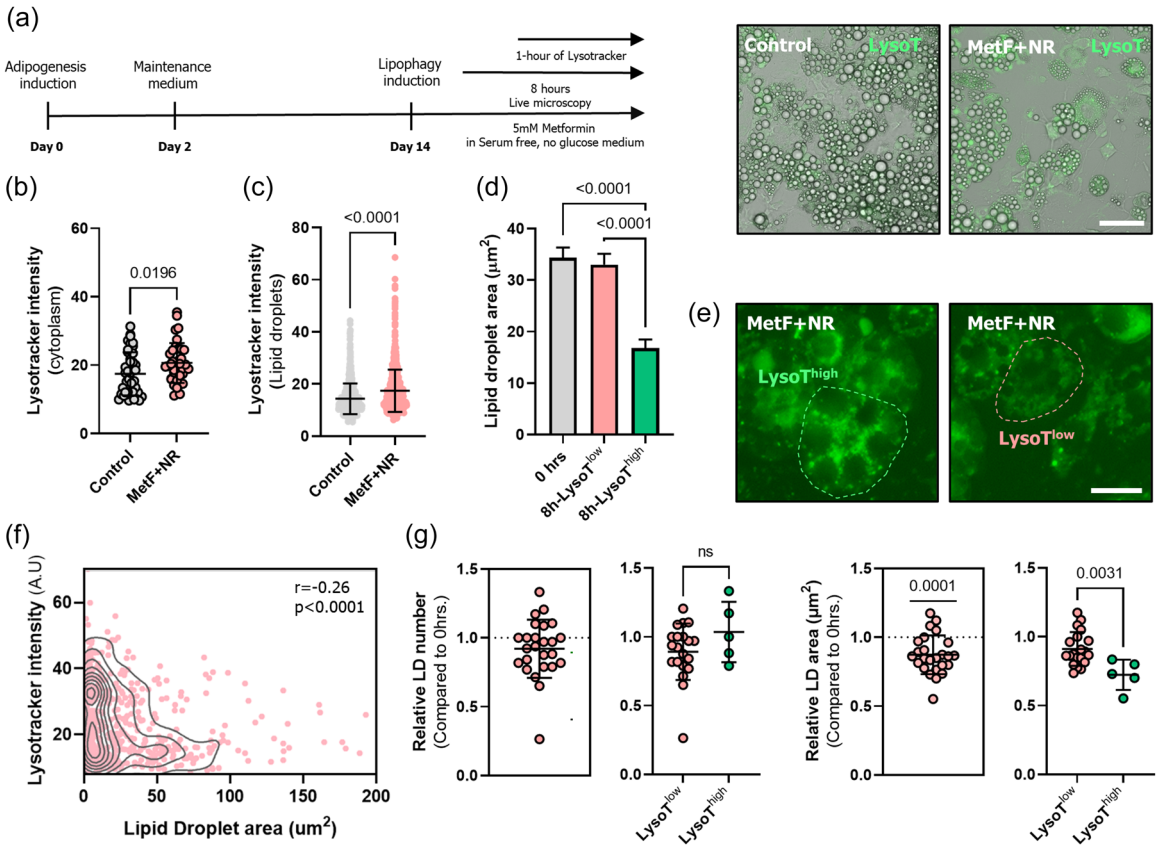

FIGURE 5 Lipid droplet (LD) analysis during acidic lipolysis. (a) Lipophagy induction experimental model and representative overlay phase-contrast images of untreated cells (Control) and metformin-treated, nutrient-starved cells (MetF+ NR) after 8 h postinduction, stained with green fluoresce lysotracker dye (magnification ×200, scale bar = 100 µm). (b) Cytoplasmatic lysotracker intensity levels in Control (gray, $n = 42$) and MetF + NR (pink, $n = 37$) treated cells after 8 h, significance was calculated using unpaired nonparametric Mann–Whitney test. (c) LD's linings lysotracker intensity analysis in Control (gray, $n = 770$) and Metformin (pink, $n = 770$), significance was calculated using unpaired nonparametric Mann–Whitney test. (d) Mean LD area after 0 (gray, $n = 571$) and 8 h of metformin and nutritional treatment in LysoT^{low} (pink, $n = 394$, LysoT intensity>40 AU) and lysoT^{high} (green, $n = 182$, LysoT intensity<40 AU), significance was calculated using unpaired one-way analysis of variance with Friedman's posttest. (e) Representative fluorescent images of MetF + NR LysoT^{low} and lysoT^{high} cells after 8 h postinduction, stained with green fluoresce lysotracker dye (magnification × 400, scale bar = 25 µm). (f) A comparison of LD's area and their respective lysotracker intensity in metformin-treated cells, the correlation was calculated using Spearman's R correlation coefficient. (g) LD area and LD number analysis after 8 h of metformin + NR relative to 0 h ($n = 25$), the cells divided to LysoT^{low} (pink) and lysoT^{high} (green) cells, significance was calculated using Wilcoxon signed-rank test and unpaired nonparametric Mann–Whitney test, respectively.

both single cell and single LDs resolutions indicating that the treatment impacted autophagy and lysosomal activity (Figure 5b,c). Next, the LDs in the MetF + NR treated cultures were separated into two groups based on the lysotracker intensity levels (40 ± AU) and compared to their initial size.

The LD area analysis revealed significant changes in the average LD area in the LysoT^{high} compared to both LysoT^{low} and the control group, with a 50% reduction (Figure 5d,e). A scattered density plot also demonstrated a negative correlation ($r = -0.26$) between the lysotracker levels in the LD surface and the respective LD's area, which indicates a possible relationship amid LD size and lysosomal activity (Figure 5f). To examine the effect of lysosomal activity on LDs dynamics, the cells were subdivided into two subpopulations based on their average LD surface lysotracker intensity levels. Interestingly, the relative number of LDs remained unchanged over time and between the groups. In contrast, the shrinkage rate of the lysoT^{high} cells was substantially higher than the lysoT^{low} cells, with a reduction of 30% in LD size compared to 10% (Figure 5g). The higher shrinkage rate in the LysoT^{high} cells demonstrates the ability of the suggested model to effectively induce and track LDs dynamics in acidic cytosolic lipolysis.

3.6 | In vivo adipocyte quantification

Based on the success of the trainable WEKA segmentation tool in identifying LDs, we have established a modified version of this workflow for in vivo whole-mounts adipose tissues. The tissues used were unstained and not fixated, thus making it a valuable tool for all adipose tissue-related experiments. In the whole mount adipose tissue, the pictures were divided into LDs content (red) and lining (green); the product was then processed several times until a

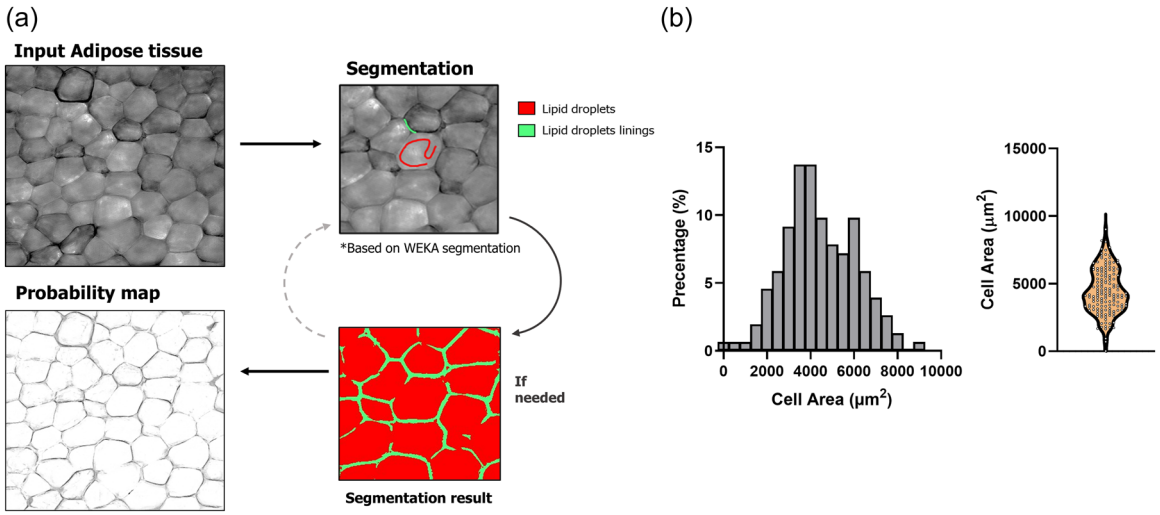

FIGURE 6 In vivo adipocyte quantification workflow. (a) Input of adipose tissue unstained whole-mount image segmentation process using waikato environment for knowledge analysis (WEKA) trainable segmentation tool. Two classes were assigned (red-cell content, green-cell linings. The classifier was trained until a satisfactory product was produced, a probability map was generated and processed using ImageJ's watershed tool. (b) A histogram and a violin plot of adipocyte cell area in whole-mount sections (n = 152).

satisfactory product was achieved (Figure 6a). The average cell area was then calculated and is showcased in a histogram and a violin plot (Figure 6b). This analysis is performed on unstained and unfixed tissues, making it a valuable and robust tool for calculating adipocyte size area in vivo that serves as a read-out of the tissue metabolic state from the mice.

4 | DISCUSSION

In the study, we described a method for quantifyingLDs size and other morphological characteristics using a machine learning segmentation tool. We present a novel workflow that allows for rapid, robust, and accurate detection and quantification of LDs in unstained images both in vitro and in vivo. This is particularly important as it enables us to track and monitor the LDs size in all cells at a single cell level and correlate it with other parameters from the same cultures, enabling us to unravel the morphological-based diversification. The method can accurately identify biogenesis, lipogenic and lipolytic dynamics over time, and hence, is instrumental in understanding how LDs respond to different molecular and chemical signals and conditions.

Image segmentation has shown great potential in processing cell images, enabling us to distinguish between our ROI from the background and other objects (Uchida, 2013). Many segmentation-based tools were developed to analyze various targets both in vitro and in vivo. In our analysis, we used the open-source program ImageJ and its plugin, named WEKA trainable segmentation. This tool is a rapid and easy-to-use plugin that combines several parameters to produce a pixel-based segmentation of images. It was used to analyze different subcellular components and compartments, including extracellular ecDNA within a glomerulus, isolating and detecting liver cells and analyzing the lipid-droplet bound mitochondria in brown adipose tissues (Ghobadi et al., 2017; Miller et al., 2021; O'sullivan et al., 2020; Ramachandran et al., 2019). While trainable WEKA segmentation was used in various systems and models, to our knowledge, a LD quantification segmentation workflow has never been described. This novel method enables us to rapidly detect LDs in high and even low-resolution images from unstained cells that are maintained in the same culture or tissue over time while yielding a more accurate result than other imaging tools.

Understanding LD dynamics through analysis of morphological attributes is of great importance as it is associated with LD dynamics evaluation and several pathological conditions (Zhang et al., 2016). Therefore, various methods have been developed over the years with the objective of quantifying LDs (Campos et al., 2018; Dejgaard & Presley, 2014; Deutsch et al., 2014; Exner et al., 2019). While some of the tools detect intracellular lipids by using lipogenic dyes that stain neutral TG and lipids, some have focused on unbiased image-processing tools for quantifying LDs in unstained images, and our group has previously presented several algorithms that detect LD in phase-contrast images (Lustig et al., 2019; Shoham et al., 2012). The significant improvement of measuring LDs using the segmentation method compared to other live-image-based tools is that it is a trainable process based on an adjustable classifier that can suit specific images with different accusation parameters. It also considers multiple parameters as a part of its analysis, which improves the accuracy and resolution for better identification of metabolic processes.

The continuous tracking of LDs allows for image-based analysis of lipogenesis and LDs catabolism in a single-cell and droplet resolution. Several pathways regulate neutral lipolysis in adipocytes. Hormonal and extracellular activation includes the β-adrenergic stimulation that triggers a cAMP-dependent cascade or the

natriuretic peptide that induces a cGMP activation pathway. These pathways trigger a set of specific and well-coordinated enzymes, named lipases, that perform triglyceride hydrolysis (Duncan et al., 2007; Yang & Mottillo, 2020). Analysis of neutral lipolysis can be performed using several different methods. Direct analysis of lipolytic activity usually measures the concentration of lipolysis products (glycerol and free fatty acids), or the triglyceride hydrolase activity. While specific, these methods do not account for the heterogenicity of LD distribution in individual cells and cannot detect multiple sub processes during the lipolysis phase (Schweiger et al., 2014). Live imaging-based methods allow for single-cell or droplet analysis that can detect the formation of micro-LD, LD fission, and LD fusion events during lipolysis (Mottillo et al., 2014; Paar et al., 2012). In our experimental conditions, the lipolytic activity was not entirely bound to a specific subpopulation as all LDs were affected, though the smaller LDs had higher lipolytic activity as they shrank at a significantly faster pace. It can be due to the subcellular position, altered dynamics, differential mechanisms, or increased surface/volume ratio that affects the distribution and density of lipolytic enzymes (Paar et al., 2012; Schott et al., 2019).

In our work, we also established a workflow based on the work of Lettieri Barbato et al. (2013) that enabled us to follow LDs dynamics during acidic lipolysis. This process is essential for maintaining LDs homeostasis; thus, tracking it is highly important in adipocytes. In contrast to neutral lipolysis, it is challenging to induce and isolate lipophagic LDs, as the droplets are morphologically identical. To account for this, we used a lysosome tracker that can follow the lysosomal activity in the cytoplasm and, more specifically, on the LDs surface (Luo et al., 2020). By combining it with metformin, which stimulates lipophagy through the activation of the AMPK pathway, and nutrient restriction, we managed to induce lysosomal-mediated LD catabolism that resulted in a differential shrinkage rate of LDs (Lettieri Barbato et al., 2013). It would be interesting to examine the changes in LD under other conditions and time durations and correlate the obtained data with different markers and labels for a more targeted single organelle analysis.

Our study supports the previous observations that showed the heterogenicity of LD diversification in individual cells. It was previously demonstrated that adipocytes could be divided into subpopulations based on their morphological appearance and their differential reaction to various stimuli (Loo et al., 2009). Recent studies also showed that adipocytes have subpopulations with distinct transcriptional signatures associated with their function in vivo and in vitro (Bäckdahl et al., 2021; Lee et al., 2019; Min et al., 2019). The single-cell resolution nature of our analysis enables us to uncover the spatial and numeric heterogeneity of the adipogenic capacity and other lipogenic functions of cells in the cultures and their relationship to other morphological characteristics. In differentiating adipocytes, cells with fewer LDs tend to have a larger average LD size, presumably through a fusion mechanism that fuses small LDs to other LD to obtain mature adipocytes eventually (Lustig et al., 2019). Indeed, in single-cell analysis, we found a strong correlation between the number of LDs in a cell and the size of the mean droplet. In the lipolytic adipocytes, the cells were divided into groups based on their initial average mean LD area. The small LD subpopulation had higher depletion and shrinkage rates compared to the other cells, with a differential lipolytic behavior. The plasticity of cellular LD storage and function stems from their size, spatial organization, associated proteins, fatty content, and intra organelles interactions (Thiam & Beller, 2017). Hence, combining our method with other image-based content-dependent techniques can elucidate LDs diversification and function.

The segmentation tool proved to be efficient in quantifying adipocyte size in vivo. Adipocyte size is a key parameter as adipose tissue dysfunction is characterized by hypertrophic adipocytes. It is also correlated with other pathophysiological conditions and is a marker for adiposity as a whole (Stenkula & Erlanson-Albertsson, 2018). Many studies have described different methods for quantitative histomorphometry of adipocytes. Fixed tissues can be stained with hematoxylin, eosin, or other markers, while the individual cells can be quantified in digested tissues (Björnheden et al., 2004; Parlee et al., 2014). We suggested a method for quantification that does not involve fixation nor digestion or other interventions that can estimate adipocytes' size using a confocal microscope. This analysis can be useful in scanning and analyzing multiple samples rapidly and accurately and correlating them with additional tools and techniques.

In conclusion, this study reveals a novel approach for quantifying LDs through supervised machine learning. The presented workflow portrays the spatial and numerical plasticity of LDs in adipose cells unbiasedly. We believe that the tool and results presented here can be implemented in different LD-related model systems that will shed light on LD diverse functions and lead to a more profound comprehension of LDs' nature and function in systemic metabolism.

AUTHOR CONTRIBUTIONS

Nadav Kislev and Dafna Benayahu conceptualized the study and developed the methodology. Nadav Kislev carried out the experiments, analyses and summarization of the results and figures. Shira Eidelheit and Shaked Perlmutter performed some of the analysis. Nadav Kislev wrote the original draft. Dafna Benayahu reviewed and edited the manuscript. All authors read and approved the final manuscript.

ACKNOWLEDGMENTS

This work was performed in partial fulfillment of the requirements for the PhD degree of Nadav Kislev, Sackler Faculty of Medicine, Tel Aviv University, Israel. Shira Eidelheit and Shaked Perlmutter are project student in the laboratory. We acknowledge Ann Avron for the editorial assistance. Nadav Kislev is an awardee of the Marian Gertner Institute for Medical Nano systems and was supported by a PhD Scholarship from the Tel Aviv University Center for Combatting Pandemics.

ORCID

Nadav Kislev https://orcid.org/0000-0002-6511-8961

REFERENCES

Arganda-Carreras, I., Kaynig, V., Rueden, C., Eliceiri, K. W., Schindelin, J., Cardona, A., & Seung, H. S. (2017). Trainable Weka Segmentation: A machine learning tool for microscopy pixel classification. *Bioinformatics*, *33*(15), 2424–2426. https://doi.org/10.1093/bioinformatics/btx180

Bäckdahl, J., Franzén, L., Massier, L., Li, Q., Jalkanen, J., Gao, H., Andersson, A., Bhalla, N., Thorell, A., Rydén, M., Ståhl, P. L., & Mejhert, N. (2021). Spatial mapping reveals human adipocyte subpopulations with distinct sensitivities to insulin. *Cell Metabolism*, *33*(9), 1869–1882. https://doi.org/10.1016/j.cmet.2021.07.018

Björnheden, T., Jakubowicz, B., Levin, M., Odén, B., Edén, S., Sjöström, L., & Lönn, M. (2004). Computerized determination of adipocyte size. *Obesity Research*, *12*(1), 95–105. https://doi.org/10.1038/oby.2004.13

Bolte, S., & Cordelières, F. P. (2006). A guided tour into subcellular colocalization analysis in light microscopy. *Journal of Microscopy*, *224*(3), 213–232. https://doi.org/10.1111/J.1365-2818.2006.01706.X

Campos, V., Rappaz, B., Kuttler, F., Turcatti, G., & Naveiras, O. (2018). High-throughput, nonperturbing quantification of lipid droplets with digital holographic microscopy. *Journal of Lipid Research*, *59*(7), 1301–1310. https://doi.org/10.1194/jlr.D085217

Dejgaard, S. Y., & Presley, J. F. (2014). New automated single-cell technique for segmentation and quantitation of lipid droplets. *Journal of Histochemistry and Cytochemistry*, *62*(12), 889–901. https://doi.org/10.1369/0022155414554835

Deutsch, M. J., Schriever, S. C., Roscher, A. A., & Ensenauer, R. (2014). Digital image analysis approach for lipid droplet size quantitation of Oil Red O-stained cultured cells. *Analytical Biochemistry*, *445*(1), 87–89. https://doi.org/10.1016/j.ab.2013.10.001

Ducharme, N. A., & Bickel, P. E. (2008). Minireview: Lipid droplets in lipogenesis and lipolysis. *Endocrinology*, *149*(3), 942–949. https://doi.org/10.1210/en.2007-1713

Duncan, R. E., Ahmadian, M., Jaworski, K., Sarkadi-Nagy, E., & Sul, H. S. (2007). Regulation of lipolysis in adipocytes. *Annual Review of Nutrition*, *27*, 79–101. https://doi.org/10.1146/annurev.nutr.27.061406.093734

Exner, T., Beretta, C. A., Gao, Q., Afting, C., Romero-Brey, I., Bartenschlager, R., Fehring, L., Poppelreuther, M., & Füllekrug, J. (2019). Lipid droplet quantification based on iterative image processing. *Journal of Lipid Research*, *60*(7), 1333–1344. https://doi.org/10.1194/jlr.D092841

Farese, R. V., & Walther, T. C. (2009). Lipid droplets finally get a little R-E-S-P-E-C-T. *Cell*, *139*(5), 855–860. https://doi.org/10.1016/j.cell.2009.11.005

Ghobadi, H., Thainimit, S., Gansawat, D., & Sugino, N. (2017). Computer-aided analysis for breast cancer detection in thermography. *2016 Management and Innovation Technology International Conference, MITiCON 2016*. MIT189–MIT192. https://doi.org/10.1109/MITICON.2016.8025216

Greenberg, A. S., Coleman, R. A., Kraemer, F. B., McManaman, J. L., Obin, M. S., Puri, V., Yan, Q. W., Miyoshi, H., & Mashek, D. G. (2011). The role of lipid droplets in metabolic disease in rodents and humans. *Journal of Clinical Investigation*, *121*(6), 2102–2110. https://doi.org/10.1172/JCI46069

Guilherme, A., Virbasius, J. V., Puri, V., & Czech, M. P. (2008). Adipocyte dysfunctions linking obesity to insulin resistance and type 2 diabetes. *Nature Reviews Molecular Cell Biology*, *9*(5), 367–377. https://doi.org/10.1038/nrm2391

Kislev, N., Izgilov, R., Adler, R., & Benayahu, D. (2021). Exploring the cell stemness and the complexity of the adipose tissue niche. *Biomolecules*, *11*(12), 1906. https://doi.org/10.3390/biom11121906

Krahmer, N., Farese, R. V., & Walther, T. C. (2013). Balancing the fat: Lipid droplets and human disease. *EMBO Molecular Medicine*, *5*(7), 973–983. https://doi.org/10.1002/emmm.201100671

Laforest, S., Labrecque, J., Michaud, A., Cianflone, K., & Tchernof, A. (2015). Adipocyte size as a determinant of metabolic disease and adipose tissue dysfunction. *Critical Reviews in Clinical Laboratory Sciences*, *52*(6), 301–313. https://doi.org/10.3109/10408363.2015.1041582

Lee, K. Y., Luong, Q., Sharma, R., Dreyfuss, J. M., Ussar, S., & Kahn, C. R. (2019). Developmental and functional heterogeneity of white adipocytes within a single fat depot. *The EMBO Journal*, *38*(3), e99291. https://doi.org/10.15252/embj.201899291

Lettieri Barbato, D., Tatulli, G., Aquilano, K., & Ciriolo, M. R. (2013). FoxO1 controls lysosomal acid lipase in adipocytes: Implication of lipophagy during nutrient restriction and metformin treatment. *Cell Death and Disease*, *4*(10), e861. https://doi.org/10.1038/CDDIS.2013.404

Listenberger, L. L., & Brown, D. A. (2007). Fluorescent detection of lipid droplets and associated proteins. *Current Protocols in Cell Biology*, *35*(1), 24.2.1–24.2.11. https://doi.org/10.1002/0471143030.cb2402s35

Loo, L. H., Lin, H. J., Singh, D. K., Lyons, K. M., Altschuler, S. J., & Wu, L. F. (2009). Heterogeneity in the physiological states and pharmacological responses of differentiating 3T3-L1 preadipocytes. *Journal of Cell Biology*, *187*(3), 375–384. https://doi.org/10.1083/jcb.200904140

Luo, X., Li, Y., Yang, P., Chen, Y., Wei, L., Yu, T., Xia, J., Ruan, X. Z., Zhao, L., & Chen, Y. (2020). Obesity induces preadipocyte CD36 expression promoting inflammation via the disruption of lysosomal calcium homeostasis and lysosome function. *EBioMedicine*, *56*, 102797. https://doi.org/10.1016/J.EBIOM.2020.102797

Lustig, M., Feng, Q., Payan, Y., Gefen, A., & Benayahu, D. (2019). Noninvasive continuous monitoring of adipocyte differentiation: From macro to micro scales. *Microscopy and Microanalysis*, *25*(1), 119–128. https://doi.org/10.1017/S1431927618015520

Miller, N., Wolf, D., Alsabeeh, N., Mahdaviani, K., Segawa, M., Liesa, M., & Shirihai, O. S. (2021). High-throughput image analysis of lipid-droplet-bound mitochondria. *Methods in Molecular Biology*, *2276*, 285–303. https://doi.org/10.1007/978-1-0716-1266-8_22

Min, S. Y., Desai, A., Yang, Z., Sharma, A., DeSouza, T., Genga, R. M. J., Kucukural, A., Lifshitz, L. M., Nielsen, S., Scheele, C., Maehr, R., Garber, M., & Corvera, S. (2019). Diverse repertoire of human adipocyte subtypes develops from transcriptionally distinct mesenchymal progenitor cells. *Proceedings of the National Academy of Sciences of the United States of America*, *116*(36), 17970–17979. https://doi.org/10.1073/pnas.1906512116

Mor-Yossef Moldovan, L., Kislev, N., Lustig, M., Pomeraniec, L., & Benayahu, D. (2020). Biomechanical stimulation effects on the metabolism of adipocyte. *Journal of Cellular Physiology*, *235*(11), 8702–8713. https://doi.org/10.1002/jcp.29714

Mor-Yossef Moldovan, L., Lustig, M., Naftaly, A., Mardamshina, M., Geiger, T., Gefen, A., & Benayahu, D. (2019). Cell shape alteration during adipogenesis is associated with coordinated matrix cues. *Journal of Cellular Physiology*, *234*(4), 3850–3863. https://doi.org/10.1002/jcp.27157

Mottillo, E. P., Paul, G. M., Moore, H. P. H., & Granneman, J. G. (2014). Use of fluorescence microscopy to probe intracellular lipolysis. *Methods in Enzymology*, *538*, 263–278. https://doi.org/10.1016/B978-0-12-800280-3.00015-3

Novikoff, A. B., Novikoff, P. M., Rosen, O. M., & Rubin, C. S. (1980). Organelle relationships in cultured 3T3-L1 preadipocytes. *Journal of Cell Biology*, *87*(1), 180–196. https://doi.org/10.1083/jcb.87.1.180

Olzmann, J. A., & Carvalho, P. (2019). Dynamics and functions of lipid droplets. *Nature Reviews Molecular Cell Biology*, *20*(3), 137–155. https://doi.org/10.1038/s41580-018-0085-z

Onal, G., Kutlu, O., Gozuacik, D., & Dokmeci Emre, S. (2017). Lipid droplets in health and disease. *Lipids in Health and Disease*, *16*(1), 128. https://doi.org/10.1186/s12944-017-0521-7

O'Sullivan, K. M., Creed, S., Gan, P. Y., & Holdsworth, S. R. (2020). Supervised machine learning for semi-quantification of extracellular DNA in glomerulonephritis. *Journal of Visualized Experiments*, *2020*(160), 1–19. https://doi.org/10.3791/61180

Paar, M., Jüngst, C., Steiner, N. A., Magnes, C., Sinner, F., Kolb, D., Lass, A., Zimmermann, R., Zumbusch, A., Kohlwein, S. D., & Wolinski, H. (2012). Remodeling of lipid droplets during lipolysis and growth in adipocytes. *Journal of Biological Chemistry*, *287*(14), 11164–11173. https://doi.org/10.1074/jbc.M111.316794

Parlee, S. D., Lentz, S. I., Mori, H., & MacDougald, O. A. (2014). Quantifying size and number of adipocytes in adipose tissue. *Methods in Enzymology*, *537*, 93–122. https://doi.org/10.1016/B978-0-12-411619-1.00006-9

Ramachandran, P., Dobie, R., Wilson-Kanamori, J. R., Dora, E. F., Henderson, B. E. P., Luu, N. T., Portman, J. R., Matchett, K. P., Brice, M., Marwick, J. A., Taylor, R. S., Efremova, M., Vento-Tormo, R., Carragher, N. O., Kendall, T. J., Fallowfield, J. A., Harrison, E. M., Mole, D. J., Wigmore, S. J., … Henderson, N. C. (2019). Resolving the fibrotic niche of human liver cirrhosis at single-cell level. *Nature*, *575*(7783), 512–518. https://doi.org/10.1038/s41586-019-1631-3

Schindelin, J., Arganda-Carreras, I., Frise, E., Kaynig, V., Longair, M., Pietzsch, T., Preibisch, S., Rueden, C., Saalfeld, S., Schmid, B., Tinevez, J. Y., White, D. J., Hartenstein, V., Eliceiri, K., Tomancak, P., & Cardona, A. (2012). Fiji: An open-source platform for biological-image analysis. *Nature Methods*, *9*(7), 676–682. https://doi.org/10.1038/nmeth.2019

Schott, M. B., Weller, S. G., Schulze, R. J., Krueger, E. W., Drizyte-Miller, K., Casey, C. A., & McNiven, M. A. (2019). Lipid droplet size directs lipolysis and lipophagy catabolism in hepatocytes. *Journal of Cell Biology*, *218*(10), 3320–3335. https://doi.org/10.1083/JCB.201803153

Schweiger, M., Eichmann, T. O., Taschler, U., Zimmermann, R., Zechner, R., & Lass, A. (2014). Measurement of lipolysis. *Methods in Enzymology*, *538*, 171–193. https://doi.org/10.1016/B978-0-12-800280-3.00010-4

Shoham, N., Gottlieb, R., Sharabani-Yosef, O., Zaretsky, U., Benayahu, D., & Gefen, A. (2012). Static mechanical stretching accelerates lipid production in 3T3-L1 adipocytes by activating the MEK signaling pathway. *American Journal of Physiology—Cell Physiology*, *302*(2), 429–441. https://doi.org/10.1152/ajpcell.00167.2011

Stenkula, K. G., & Erlanson-Albertsson, C. (2018). Adipose cell size: Importance in health and disease. *American Journal of Physiology—Regulatory Integrative and Comparative Physiology*, *315*(2), R284–R295. https://doi.org/10.1152/ajpregu.00257.2017

Tang, Q. Q., & Lane, M. D. (2012). Adipogenesis: From stem cell to adipocyte. *Annual Review of Biochemistry*, *81*, 715–736. https://doi.org/10.1146/annurev-biochem-052110-115718

Thiam, A. R., & Beller, M. (2017). The why, when and how of lipid droplet diversity. *Journal of Cell Science*, *130*(2), 315–324. https://doi.org/10.1242/jcs.192021

Uchida, S. (2013). Image processing and recognition for biological images. *Development Growth and Differentiation*, *55*(4), 523–549. https://doi.org/10.1111/dgd.12054

Yang, A., & Mottillo, E. P. (2020). Adipocyte lipolysis: From molecular mechanisms of regulation to disease and therapeutics. *Biochemical Journal*, *477*(5), 985–1008. https://doi.org/10.1042/BCJ20190468

Zechner, R., Madeo, F., & Kratky, D. (2017). Cytosolic lipolysis and lipophagy: Two sides of the same coin. *Nature Reviews Molecular Cell Biology*, *18*(11), 671–684. https://doi.org/10.1038/nrm.2017.76

Zhang, S., Wang, Y., Cui, L., Deng, Y., Xu, S., Yu, J., Cichello, S., Serrero, G., Ying, Y., & Liu, P. (2016). Morphologically and functionally distinct lipid droplet subpopulations. *Scientific Reports*, *6*(1), 1–14. https://doi.org/10.1038/srep29539

SUPPORTING INFORMATION

Additional supporting information can be found online in the Supporting Information section at the end of this article.

How to cite this article: Kislev, N., Eidelheit, S., Perlmutter, S., & Benayahu, D. (2022). How to follow lipid droplets dynamics during adipocyte metabolism. *Journal of Cellular Physiology*, 237, 4157–4168. https://doi.org/10.1002/jcp.30857